Appl Phys A (2009) 96: 403–408
DOI 10.1007/s00339-009-5186-2

Applied Physics A
Materials Science & Processing

RAPID COMMUNICATION

Stranski–Krastanov growth of InGaN quantum dots emitting in green spectra

C. Bayram · M. Razeghi

Received: 6 February 2009 / Accepted: 3 March 2009 / Published online: 17 March 2009
© Springer-Verlag 2009

Abstract Self-assembled InGaN quantum dots (QDs) were grown on GaN templates by metalorganic chemical vapor deposition. 2D–3D growth mode transition through Stranski–Krastanov mode was observed via atomic force microscopy. The critical thickness for $In_{0.67}Ga_{0.33}N$ QDs was determined to be four monolayers. The effects of growth temperature, deposition thickness, and V/III ratio on QD formation were examined. The capping of InGaN QDs with GaN was analyzed. Optimized InGaN quantum dots emitted in green spectra at room temperature.

PACS 81.15.Gh · 81.16.Dn · 81.07.Ta · 78.66.Fd

1 Introduction

Solid state lighting (SSL) holds the promise of a more energy-efficient, longer-lasting, more compact, and lower maintenance substitute for today's incandescent and fluorescent light sources. Since lighting currently represents about 22% of all electricity consumption, the adoption of SSL could significantly reduce greenhouse gas emissions [1]. Light-emitting diodes (LEDs) based on the InGaN alloy are currently the most promising candidates for realizing SSL. InGaN is a direct wide-band-gap semiconductor with an emission that can span the entire visible spectra via compositional tuning.

C. Bayram · M. Razeghi (✉)
Center for Quantum Devices, Department of Electrical Engineering and Computer Science, Northwestern University, 2220 Campus Drive, Room 4051, Evanston, IL 60208, USA
e-mail: razeghi@eecs.northwestern.edu
Fax: +1-847-467-1817

With increasing indium content (from violet to green emission) a significant decrease in performance is observed in light emitters based on quantum wells [2, 3]. One of the crucial reasons is that the large lattice mismatch between high indium content InGaN and GaN induces the generation of dislocations in the active region [2–4]. This explains how the performance decreases for high indium content light emitters, even on low-dislocated templates [3, 5, 6]. The use of quantum dots may be one way to overcome these limitations in high-indium-content devices. Strain due to high indium content can be channeled into quantum dot (QD) formation which can decrease the overall strain otherwise which would form dislocations [7]. Besides, optoelectronic devices based on QDs have many advantages over those based on QWs, such as temperature stability and higher efficiency [8].

Room temperature blue emission from QDs was reported earlier [9, 10]. The strong luminescence from these QDs was attributed to the exitonic transitions [11]. The blue QDs have been integrated into LEDs [12]. However, there are few studies of InGaN quantum dots in the green spectra [13]. In this work, we study the formation of high-indium-content InGaN QDs, and study the effect of growth temperature, deposition thickness and V/III ratio on QD formation. We also report the stability of GaN capped InGaN QDs grown by Stranski–Krastanov (SK) mode.

2 Experiment

The samples are grown in an AIXTRON 200/4-HT horizontal flow, low-pressure metalorganic chemical vapor deposition (MOCVD) reactor. Trimethylgallium (TMGa) and trimethlyindium (TMIn) are the metalorganic cation precursors for Ga and In sources, respectively. Ammonia (NH_3)

is used as the nitrogen source. All QD growths are realized under N_2 to facilitate the incorporation of indium.

The InGaN layers were grown on 2-µm-thick GaN on double side polished (DSP) (0001) sapphire (Al_2O_3) substrate. The growth rate was 11.8 Å/min and growth was interrupted for 15 s under ammonia before cool down. We studied the effect of temperature, deposition thickness, and V/III ratio on the formation and optical quality of the InGaN QDs.

3 Result and discussion

Atomic force microscopy (AFM) was used to study the QD formation. Figures 1a, b, c displays the (1 µm × 1 µm) AFM images of 5.8 monolayer (ML) InGaN grown at 734°C, 679°C, and 633°C, respectively (1 ML ≅ 2.7 Å). At 734°C, as seen in Fig. 1a, only island like 2-D quantum disks (Q-disks) formed. Lowering the growth temperature (Ts) further resulted in smaller disks and surface roughening (Fig. 1b). This behavior was attributed to the decrease in adatom mobility and increase in the indium content of Q-disks. The adatom mobility decreased as a result of lowered Ts, and indium content increased due to higher indium thermodynamic equilibrium at low temperatures. Effecting both the thermodynamic (indium content in InGaN) and kinetic (mobility) equilibrium on the surface, temperature is observed to be the most crucial parameter of high-quality QD growths. We have determined 633°C to be a proper growth temperature for green emitting InGaN QDs.

Figures 2a, b, c displays the (1 µm × 1 µm) AFM images of 2.9-, 4.4-, and 5.8-ML-thick InGaN grown at 633°C, respectively. At this Ts, critical thickness for QD formation is determined to be ∼4.0 ML. Below the critical thickness, no QDs are observed (and the surface is similar to Fig. 2a). Above critical thickness, increasing the deposited InGaN results in increase in the density of the QDs in the expense of uniformity (Figs. 2b, c).

The effect of V/III ratio on the surface morphology is studied. Figure 3 displays the AFM root-mean-square (RMS) roughness (1 µm × 1 µm) of 4.0 ML InGaN layer with respect to V/III ratio at Ts of 633°C. For this deposition thickness and temperature no QDs are observed. As seen in Fig. 3, V/III ratio strongly effects the surface roughness. We have determined 13.88×10^3, where the roughness is maximized in Fig. 3, to be a proper V/III ratio for QD formation at 633°C.

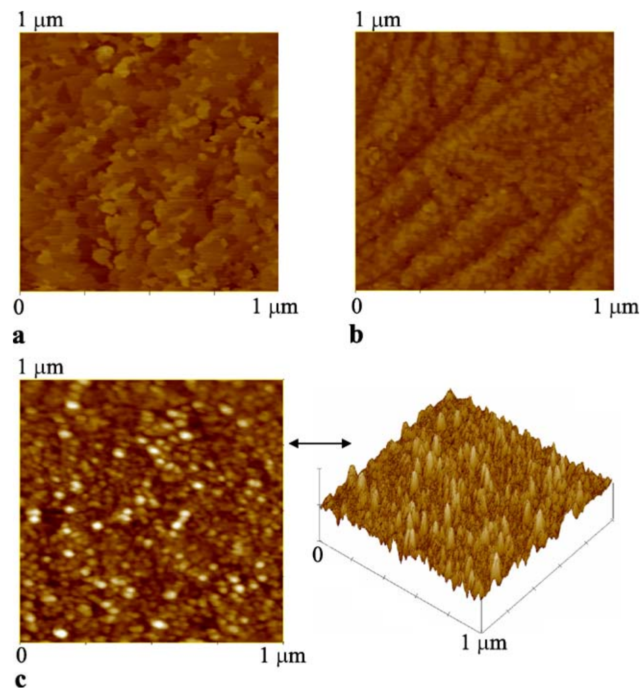

Fig. 1 AFM (1 µm × 1 µm) images of 5.8 ML InGaN grown at **a** $T = 734$°C, **b** $T = 679$°C, and **c** $T = 633$°C

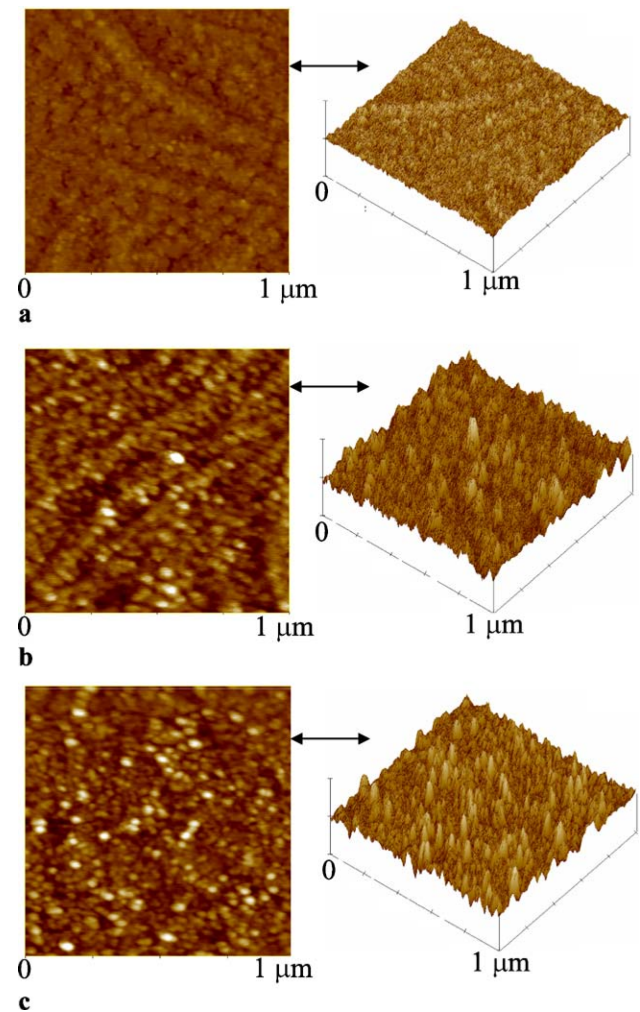

Fig. 2 AFM (1 µm × 1 µm) images of **a** 2.9 ML, **b** 4.4 ML, and **c** 5.8 ML InGaN grown at $T = 633$°C

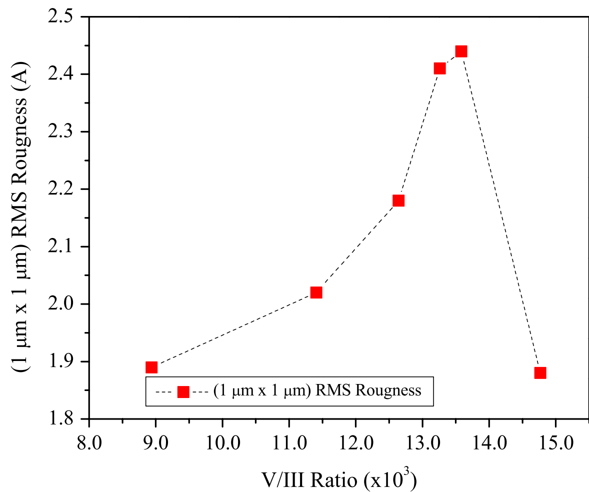

Fig. 3 AFM RMS roughness (1 μm × 1 μm) versus V/III ratio for 4.0 ML InGaN grown at $T = 633°\mathrm{C}$

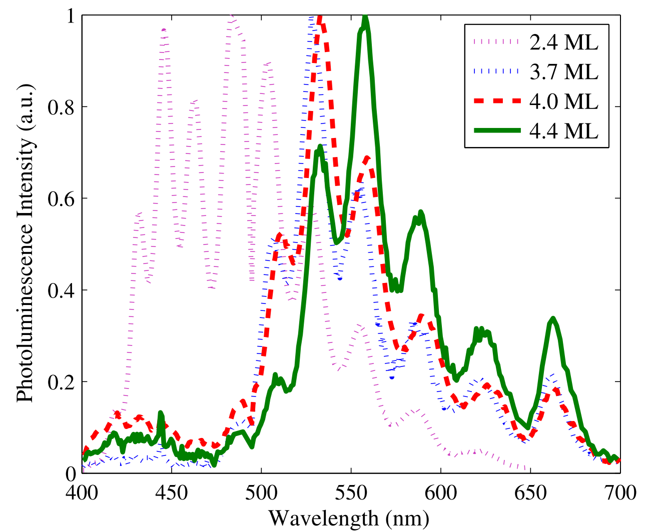

Fig. 5 Normalized photoluminescence intensity versus wavelength at room temperature for 2.4-, 3.7-, 4.0-, and 4.4-ML-thick InGaN

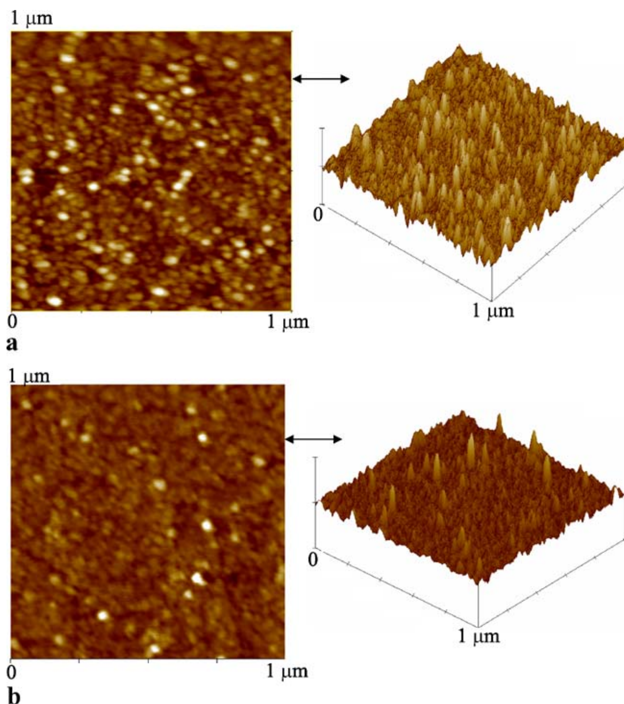

Fig. 4 AFM (1 μm × 1 μm) images of 5.8 ML InGaN grown at $T = 633°\mathrm{C}$ with V/III ratio **a** 13.88×10^3, and **b** 13.57×10^3

Effect of V/III ratio on QD formation is studied separately. Figures 4a, b displays the (1 μm × 1 μm) AFM images of 5.8-ML-thick InGaN grown at 633°C with V/III ratio being 13.88×10^3 and 13.57×10^3, respectively. As seen, higher V/III ratio results in bigger quantum dots, similar to increased RMS roughness in Fig. 3. V/III ratio being 13.88×10^3, increasing or decreasing V/III ratio results in less uniform quantum dots. Thus, we have kept the V/III ratio at 13.88×10^3 thereafter.

Maintaining the growth temperature at 633°C, and V/III ratio at 13.88×10^3, we have identified formation of two different quantum structures: quantum disks and quantum dots. When InGaN is deposited less than critical thickness of 4 ML, some kind of 2-D structure similar to Fig. 2a was observed. As the height of these structures were much smaller than their width (as observed via AFM analyses), they are referred to as quantum disks. Deposited more than 4 ML, QD formation was observed via AFM (Figs. 2b, c).

The photoluminescence of the InGaN quantum structures were studied at room temperature (Fig. 5) via 244 nm line of Argon laser. Due to low excitation (18 $\mathrm{W/cm^2}$), the main transition in QDs is from ground levels of conduction and valance bands. Fabry–Perot reflections (in Fig. 5) are observed due to 2-μm-thick GaN cavity. At 558 nm calculated Fabry–Perot peak separation is 34 nm not far from what we experimentally observe.

At our optimized growth conditions, InGaN relaxes into two different quantum structures, quantum disks or quantum dots depending on the deposited thickness. For ∼2.4 ML InGaN deposition, the layer is pseudomorphic, and broad band emission from 420 to 520 nm is observed. For InGaN deposition ≥3 ML, the layer tends to partially relax by forming quantum disks, as shown in Fig. 2a, which leads to two distinct PL bands in Fig. 5. The first band (420–460 nm) presenting a low PL emission intensity is attributed to a wetting layer. The existence of this wetting layer is due to SK mode. The high-intensity band has a peak at 525 nm and corresponds to emission from the (higher indium content) quantum disks. At a thickness of 4.4 ML, quantum dot formation occurs, as shown in Fig 2b. Two PL bands are also observed, but the high-indium-content band corresponding to QD emission has a longer wavelength (558 nm) than that of the quantum disk. In conclusion, QD formation takes

Fig. 6 AFM Surface Plot for **a** 2 nm capped (1 μm × 1 μm), **b** 5 nm capped (5 μm × 5 μm) 4.4 ML InGaN QDs. **c** Peak photoluminescence intensity dependence on capping thickness

place after deposition of critical thickness of about 4.0 ML with an apparent PL redshift. When 4.4 ML InGaN is deposited, the average size of the quantum dots are 0.8 nm in height and 36 nm in bottom diameter, and their density is $1 \times 10^{10}\ \text{cm}^{-2}$.

In Ref. [14], the detrimental effect of quantum dot height on radiative lifetime is reported. The strong room temperature luminescence of our QDs should be due to smaller QD height leading to a higher overlap between electron and hole wavefunctions. Thus, achieving high-optical-quality InGaN QDs requires precise control of the InGaN growth rate and is attainable at low growth rates via MOCVD.

Integrating the QDs in LEDs requires an appropriate means of capping. A low-temperature GaN capping layer is investigated to cap 4.4 ML InGaN QDs. For a 2-nm-thick capping layer we can still resolve the QDs by AFM (Fig. 6a). However, with 5-nm-thick capping, the QDs are completely covered (Fig. 6b). The PL intensity dependence on capping thickness is shown in Fig. 6c. When just covered, the PL intensity increases. However, a thicker capping layer reduces the emission intensity possibly due to the absorption losses in the thick GaN capping layer.

4 Calculation of the indium content

Iterative calculation of strain and piezoelectric effects on the band gap are used along with ground energy levels to estimate the indium content of the InGaN QDs using experimental PL data as input. The set of parameters used in this work could be found in Ref. [15]. Vegard's Law is used to interpolate values for $\text{In}_x\text{Ga}_{(1-x)}\text{N}$.

The InGaN QDs are known to have trapezoidal shape, which can be observed via transmission electron microscope studies [16]. Thus, InGaN QDs are assumed to have a trapezoidal shape with 35° side wall angle while calculating the ground state energies by finite-element modeling (FEM).

The relation between band gap determined from PL(E_{g}^{PL}) and real compositional band gap (E_{g}^{x}) is approximated as follows:

$$E_{\text{g}}^{\text{PL}} = E_{\text{g}}^{x} + E_{x}^{\text{g–g}} + \Delta E_{\text{g}} \tag{1}$$

where strain and piezoelectric field effects are included in ΔE_{g}. $E_{x}^{\text{g–g}}$ is the sum of the conduction and valance band ground energy levels relative to their respective bands. Finite-element modeling is used to calculate the ground energy levels of the quantum dots. Assuming an initial indium composition, $E_{x}^{\text{g–g}}$ and ΔE_{g} is calculated giving E_{g}^{x}. From this result of E_{g}^{x} the new indium content (x_{In}) and the new value for strain and ground states are calculated. This new strain and ground state transition energy lead to a new E_{g}^{x}. Iteration continues until indium content (x_{In}) converges.

The band gap of the InGaN is calculated from

$$E_{\text{g}}^{x} = x_{\text{Ga}} E_{\text{g}}^{\text{GaN}} + x_{\text{In}} E_{\text{g}}^{\text{InN}} - b x_{\text{Ga}} x_{\text{In}} \tag{2}$$

where $b = 2.77/(1 + 1.007 x_{\text{In}})$ gives indium content dependent InGaN bowing parameter to match experimental data [17]. The effect of strain and piezoelectric effect on band gap at room temperature can be calculated by separating the effect of strain (ϵ) and piezoelectric fields (QCSE) as follows:

$$\Delta E_{\text{g}} = \Delta E_{\text{g}}^{\epsilon} + \Delta E_{\text{g}}^{\text{QCSE}} \tag{3}$$

As only the lowest possible transition in room temperature is of interest, the total change in band gap due to strain could be written as sum of the contributions from change in conduction and valance (heavy hole) bands, as in (4).

$$\Delta E_{\text{g}}^{\epsilon} = \Delta E_{\text{c}}^{\epsilon} - \Delta E_{\text{v,hh}}^{\epsilon} \tag{4}$$

For pseudomorphic wurtzite films grown along (0001) z-axis, the nonzero strain elements are [18]

$$\epsilon_{xx} = \epsilon_{yy} = \frac{c_{\text{GaN}} - c_{\text{InGaN}}}{c_{\text{InGaN}}} \tag{5}$$

$$\epsilon_{zz} = -\frac{2C_{13}}{C_{33}} \epsilon_{xx} \tag{6}$$

where c is the in-plane lattice constant and C_{ij} is the elastic constant.

The change in conduction band due to strain ($\Delta E_{\text{c}}^{\epsilon}$) is calculated [19, 20] as

$$\Delta E_c^\epsilon = a_c^z \Delta\epsilon_{zz} + a_c^{x,y}(\Delta\epsilon_{xx} + \Delta\epsilon_{yy}) \tag{7}$$

$$= a_c^z\left(-\frac{2C_{13}}{C_{33}}\Delta\epsilon_{xx}\right) + a_c^{x,y}(2\Delta\epsilon_{xx}) \tag{8}$$

where a_c^z, and $a_c^{x,y}$ are hydrostatic deformation potential constants.

The calculation [18, 20] of valance band shift due to strain is as follows:

$$\Delta E_{v,hh}^\epsilon = \lambda_\epsilon + \theta_\epsilon \tag{9}$$

$$\lambda_\epsilon = D_1\Delta\epsilon_{zz} + D_2(\Delta\epsilon_{xx} + \Delta\epsilon_{yy}) \tag{10}$$

$$\theta_\epsilon = D_3\Delta\epsilon_{zz} + D_4(\Delta\epsilon_{xx} + \Delta\epsilon_{yy}) \tag{11}$$

where D_1, D_2, D_3, and D_4 are deformation potential constants. By using (4, 7, 9) the effect of strain on the band gap (ΔE_g^ϵ) is calculated for any indium content in InGaN. Our result agrees that increasing the compressive strain ($\Delta\epsilon_{xx} < 0$) increases the band gap.

Polarization related electric field has two components: spontaneous and strain induced. Spontaneous component is independent of the strain and dependent on the composition. Strain induced one depends on composition via strain.

Piezoelectric field is calculated from surface charge density. The surface charge density for both components can be calculated as [21, 22]:

$$\sigma^z = \sigma_{st}^z + \sigma_{sp}^z \tag{12}$$

$$\sigma_{st}^z = 2\,\epsilon_{xx}\left(e_{31} - e_{33}\frac{C_{13}}{C_{33}}\right) \tag{13}$$

$$\sigma_{sp}^z = x_{Ga}P_{GaN}^{sp} + x_{In}P_{InN}^{sp} \tag{14}$$

where P_{AN}^{sp} is the spontaneous polarization coefficient of binary compound AN. Piezoelectric field (ε^{PE}) follows the charge density as:

$$\varepsilon^{PE} = \frac{\sigma^z}{2\epsilon_0\epsilon_r} \tag{15}$$

where ϵ_0 and ϵ_r are the vacuum and relative permittivity constants. Thus change in the band gap due to electric field, quantum-confined Stark effect (QCSE), could be approximated as [23]:

$$\Delta E_g^{QCSE} = \frac{C_1(m_e^* + m_h^*)m_0 e^2\varepsilon^2 L_{eff}^4}{\hbar^2} \tag{16}$$

where $C_1 = -2.19 \times 10^{-3}$ and $L_{eff} = 8 \times 10^{-10}$ m are used. m_0 is the electron mass, e is the unit charge, and $\hbar$ is the Planck's constant over 2π. m_e and m_h are the effective masses of the electron and heavy hole, respectively. L_{eff} is the effective thickness, and assumed to be the biggest QD height not to underestimate the change in the band gap due to electric field (ΔE_g^{QCSE}). ε is the electric field due to spontaneous and strain-induced charges. From (16), decreasing the electric field results in a larger band gap, as expected.

By using (8, 9, 16) in (17)

$$\Delta E_g = \left(\Delta E_c^\epsilon - \Delta E_{v,hh}^\epsilon\right) + \Delta E_g^{QCSE} \tag{17}$$

and iterating, indium content is determined to be 67.4% resulting a strain of −6.3%. The minus sign of strain indicates compressive nature. Due to small height of QDs, change in band gap due to electric field (∼3.3 MV/cm) is on the order of −2.0 meV whereas change in band gap due to strain is 78.4 meV. The signs indicate the opposing processes. Thus, in QDs the effect of strain on band gap is dominant rather than that of piezoelectric fields. From FEM simulations, the converged ground energy levels of 0.217 eV for conduction band and 0.158 eV for valance band (measured from their respective bands) are reached as for $In_{0.67}Ga_{0.33}N$ QDs.

In quantum-well-based nitride light emitters, the emission blue shifts with increasing injection current due to free-carrier screening that occurs due to the high piezoelectric field [6, 24]. This injection-dependent wavelength shift is undesirable for lasers as the gain structure is typically optimized for a single wavelength. Thus, QDs band gap being less affected by electric field should help more wavelength-stable emission in nitride light emitters. As InGaN is sensitive to regrowth of GaN at high temperatures, these QDs could be particularly beneficial in hybrid structures [3] that employs ZnO layers grown atop of InGaN QDs at lower temperatures than that of (In)GaN layers.

5 Conclusion

Stranski–Krastanow growth of InGaN quantum dots (QDs) on GaN templates are realized. Effect of growth temperature, deposition thickness and V/III ratio on QD formation are studied. InGaN QDs with a peak emission wavelength of 558 nm at room temperature are realized. These QDs are capped to be integrated into optoelectronic devices. Theoretical analysis suggests that due to low QD height, piezoelectric field effect on band gap is small which should lead to more stable emission wavelength with injection current. InGaN QDs promises applications in conventional and hybrid green-light emitters.

Acknowledgements The authors acknowledge useful discussions with Stanley Tsao, Ho-Chul Lim, and Dr. Wei Zhang regarding quantum dot growth, Dr. T. Yamanaka regarding finite-element modeling of QDs, and Dr. B. Movaghar for valuable discussions, all from Center for Quantum Devices, Northwestern University, IL, USA.

References

1. C.J. Humphreys, MRS Bull. **33**, 459 (2008)

2. Y. Cho, S.K. Lee, H.S. Kwack, J.Y. Kim, K.S. Lim, H.M. Kim, T.W. Kang, S.N. Lee, M.S. Seon, O.H. Nam, Y.J. Park, Appl. Phys. Lett. **83**, 2578 (2003)
3. C. Bayram, F.H. Teherani, D. Rogers, M. Razeghi, Appl. Phys. Lett. **93**, 081111 (2008)
4. F.A. Ponce, S. Srinivasan, A. Bell, L. Geng, R. Liu, M. Stevens, J. Cai, H. Omiya, H. Marui, S. Tanaka, Phys. Status Solidi **240**, 273 (2003)
5. T. Kozaki, H. Matsumura, Y. Sugimoto, S. Nagahama, T. Mukai, Proc. SPIE **6133**, 613306 (2006)
6. C. Bayram, J.L. Pau, R. McClintock, M. Razeghi, Appl. Phys. B (2008). doi:10.1007/s00340-008-3321-y
7. D.J. Eaglesham, M. Cerullo, Phys. Rev. Lett. **64**, 1943 (1990)
8. M. Petroff, A. Lorke, A. Imomoglu, Phys. Today **54**, 46 (2001)
9. K. Tachibana, T. Someya, Y. Arakawa, Appl. Phys. Lett. **74**, 383 (1999)
10. B. Damilano, N. Grandjean, S. Dalmasso, J. Massies, Appl. Phys. Lett. **75**, 3751 (1999)
11. O. Moriwaki, T. Someya, K. Tachibana, S. Ishida, Y. Arakawa, Appl. Phys. Lett. **76**, 2361 (2000)
12. Y.K. Su, S.J. Chang, L.W. Ji, C.S. Chang, L.W. Wu, W.C. Lai, T.H. Fang, K.T. Lam, Semicond. Sci. Technol. **19**, 389 (2004)
13. S. Choi, J. Jang, S. Yi, J. Kim, W. Jung, Proc. SPIE **6479**, 64791F (2007)
14. V. Ranjan, G. Allan, C. Priester, C. Delerue, Phys. Rev. B **68**, 115305 (2003)
15. I. Vurgaftman, J.R. Meyer, L.R. Ram-Mohan, Appl. Phys. Rev. **89**, 5815 (2001)
16. K.S. Kim, C.H. Hong, W.H. Lee, C.S. Kim, O.H. Cha, G.M. Yang, E.K. Suh, K.Y. Lim, H.J. Lee, H.K. Cho, J.Y. Lee, J.M. Seo, MRS Int. J. Nitride Semicond. Res. **5S1**, W11.74 (2000)
17. M. Androulidaki, N.T. Pelekanos, K. Tsagaraki, E. Dimakis, E. Iliopoulos, A. Adikimenakis, E. Bellet-Amalric, D. Jalabert, A. Georgakilas, Phys. Status Solidi **6**, 1866 (2006)
18. S.L. Chuang, C.S. Chang, Phys. Rev. B **54**, 2491 (1996)
19. M. Grundmann, O. Stier, D. Bimberg, Phys. Rev. B **52**, 11969 (1995)
20. C.G. Van de Walle, M.D. McCluskey, C.P. Master, L.T. Romano, N.M. Johnson, Mat. Sci. Eng. B **59**, 274 (1999)
21. O. Ambacher, J. Majewski, C. Miskys, A. Link, M. Hermann, M. Eicjkhoff, M. Stutzmann, F. Bernardini, V. Fiorentini, V. Tilak, B. Schaff, L.F. Eastman, J. Phys. Condens. Matter **14**, 3399 (2002)
22. V.A. Fonoberov, A.A. Balandin, J. Appl. Phys. **94**, 7178 (2003)
23. S.L. Chuang, *Physics of Optoelectronic Devices* (Wiley, New York, 1995)
24. S. Chichibu, T. Azuhata, T. Sota, S. Nakamura, Appl. Phys. Lett. **69**, 4188 (1996)